ORGANOMETALLICS

Article

pubs.acs.org/Organometallics

Charge-Delocalized κ^2C,N-NHC-Amine Complexes of Rhodium, Iridium, and Ruthenium

Eveline Jansen,[†] Martin Lutz,[‡] Bas de Bruin,*[,†] and Cornelis J. Elsevier*[,†]

[†]Van 't Hoff Institute for Molecular Chemistry, University of Amsterdam, Science Park 904, 1098 XH Amsterdam, The Netherlands

[‡]Bijvoet Center for Biomolecular Research, Crystal and Structural Chemistry, Faculty of Science, Utrecht University, Padualaan 8, 3584 CH Utrecht, The Netherlands

Supporting Information

ABSTRACT: The development of a novel set of complexes bearing an NHC-amine ligand (C^{NHC}-NH_2) is described. M(cod) complexes (M = Ir, Rh) and a Ru complex have been synthesized in which three different coordination modes of the ligand were established: monodentate, neutral bidentate, and anionic bidentate. The anionic bidentate coordination mode of the anionic C^{NHC}-NH^- ligand arises from deprotonation of the amine moiety of the neutral C^{NHC}-NH_2 ligand. Ligand deprotonation proved to be reversible for the Rh and Ir complexes, as was shown by subsequent treatment of the complexes with base and acid. The structural parameters of these differently coordinated ligands were examined, and it was shown that the conjugation of the aniline ring plays a major role in determining the ligand properties. Structural parameters derived from DFT calculations confirm delocalization of the anionic charge over the ligand framework, as is clear from a comparison of the (hypothetical) neutral bidentate complexes $[M(cod)(\kappa^2C,N\text{-}\{C^{NHC}\text{-}NH_2\})]^+$ with those of the (synthesized) monoanionic complexes $[M(cod)(\kappa^2C,N\text{-}\{C^{NHC}\text{-}NH\})]$ (M = Rh, Ir). A similar trend in the structure and bond lengths of the aniline rings was found in the solid-state structure of the novel dimeric complex $[(Ru(\kappa^2C,N\text{-}\{C^{NHC}\text{-}NH\})(\kappa^2C,N\text{-}\{C^{NHC}\text{-}NH_2\})Cl)_2(\mu\text{-}Cl)](PF_6)$. The octahedral d^5 ruthenium(III) centers in this complex both contain a neutral bidentate C^{NHC}-NH_2 ligand as well as an anionic bidentate C^{NHC}-NH^- ligand. Quite remarkably, the complex is diamagnetic, arising from antiferromagnetic coupling of the two low-spin ruthenium(III) centers over the chloride linker. DFT calculations indeed confirm that the open-shell singlet electronic structure is most stable.

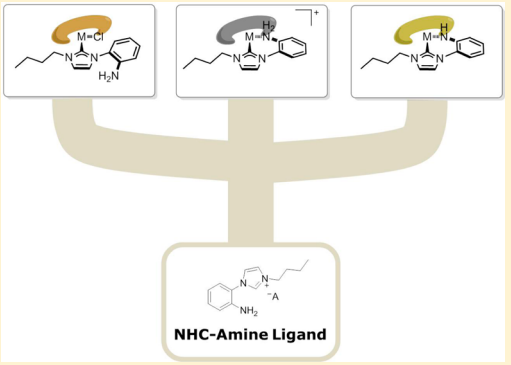

INTRODUCTION

The use of carbenes as ligands is well developed in the field of transition-metal complex chemistry.[1] In particular, the N-heterocyclic carbene (NHC) class of imidazol-2-ylidines, first reported in the 1960s,[2] have received their fair share of attention. Many successful examples of the application of NHCs in transition-metal-catalyzed transformations such as hydrogenations and metathesis reactions[3−5] have been reported. We recently reported on the synthesis of a conjugated NHC-amine ligand species where an NHC is conjugated with an aniline (C^{NHC}-NH_2).[6] In this species, the primary amine is tethered to the NHC via an aromatic ring. The amine moiety of our C^{NHC}-NH_2 ligand **A** (see Figure 1) can coordinate in a neutral or in an anionic fashion (when deprotonated). Monoanionic (bidentate) ligands have found widespread application in homogeneous catalysis. The most recognized are (pentamethyl)cyclopentadienyl (Cp, Cp*), acetylacetonate (acac), and diketimine (nacnac, where the two oxygen atoms of acac have been replaced by nitrogen-based moieties of the form NR).[7,8] Well-known examples of bifunctional ligands are ligands containing hydroxyl or oxime[9] groups and pincer-type ligands containing an anionic donor arm.[10,11] Previous work by Morris, involving a benzylic amine tethered to an NHC, has shown the ability of this ligand scaffold to display cooperativity, but this depended greatly on other factors such as the ancillary ligand (*p*-cym vs Cp*) and solvent assistance.[12] Morris also explored the potential of iridium(I)-cod complexes containing neutral bidentate NHC-benzylic amine ligands, coordinated as seven-membered chelate rings to the metal center. Aniline-based C^{NHC}-NH_2 ligands, forming neutral complexes containing conjugated anionic C^{NHC}-NH^- ligands bound to Rh, Ir, or

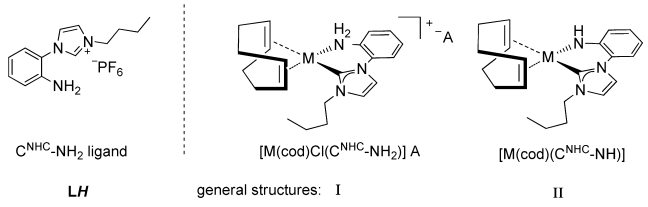

Figure 1. C^{NHC}-NH_2 ligand (**L*H***) and the general structure of the complexes we aimed to develop. The general structure **I** contains the neutral C^{NHC}-NH_2 ligand **L*H***, while the general structure **II** contains the monoanionic (deprotonated) C^{NHC}-NH^- ligand $\mathbf{L}^-$.

Received: April 4, 2014
Published: May 22, 2014

   dx.doi.org/10.1021/om5003599 | *Organometallics* 2014, 33, 2853−2861

Ru as six-membered chelate rings, have thus far remained unreported. We became interested in the possible coordination modes and potential cooperative effects of such C^{NHC}-NH_2 ligands. Previously we found that the small chelate ring size that is present in our C^{NHC}-NH_2 ligand, together with the conjugated structure, renders the NHC carbene more electron rich in comparison to the larger NHC-benzylic amine analogue. This markedly improved the catalytic activity for complexes that preferred to follow an inner-sphere coordination pathway (without bifunctional behavior of the ligand) in the hydrogenation of polar bonds. For complexes following an outer-sphere pathway, the different structural parameters were of minor influence.

Herein we report a set of novel Ru, Ir, and Rh complexes, bearing the C^{NHC}-NH_2 ligand **L*H*** and the monoanionic C^{NHC}-NH^- ligand $\mathbf{L}^-$ (formed by amine deprotonation of **L*H***), with **L*H*** binding in different coordination modes (Figure 1). We focus in particular on the influence of the anionic ligand charge (in $\mathbf{L}^-$) on the structural parameters of the complex.

The synthesis, characterization, and structural parameters of M(cod) complexes (M = Rh, Ir) of general structures **I** and **II** are discussed. Additionally, we report an unusual dinuclear, diamagnetic *bis*-ruthenium(III) species, having both a neutral C^{NHC}-NH_2 ligand **L*H*** and an anionic C^{NHC}-NH^- ligand $\mathbf{L}^-$ bound to each ruthenium(III) center. This complex appears to have an open-shell singlet ground state, resulting in antiferromagnetic coupling between the two $S = {}^1/_2$ ruthenium centers.

RESULTS AND DISCUSSION

Synthesis of [M(cod)Cl(κ^1-*C*-{C^{NHC}-NH_2})] (M = Ir, Rh) Complexes 1 and 2. We first aimed to synthesize the complexes of general structure **I** by building on published procedures for the coordination of an NHC-bidentate ligand to form an [M(cod)L] complex.[13,14] Complex **1** was synthesized by first reacting $[Ir(cod)Cl]_2$ with KO*t*Bu to form an alkoxide-bridged metal precursor (Scheme 1). The alkoxide ligand of this precursor was used as an internal base for the imidazolium PF_6 salt added subsequently to coordinate the NHC ligand (route *A*). This is a general approach for the synthesis of M-NHC complexes for a variety of metals.[15] Subsequent work-up yielded [Ir(cod)(κ^1*C*-{C^{NHC}-NH})] complex **1** as a yellow powder in 53% yield. Spectroscopic analysis of complex **1** thus obtained revealed that the C^{NHC}-NH_2 ligand acts as a monodentate ligand. The metal apparently prefers coordination of a chloride over coordination of the primary amine of ligand **L*H***.

Scheme 1. Formation of [M(cod)Cl(κ^1*C*-{C^{NHC}-NH_2})] Complexes 1 and 2 (M = Ir, Rh)[a]

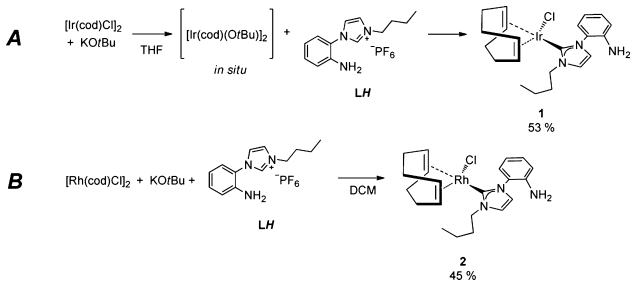

[a]Route *A* shows the preformation of the $[Ir(cod)(OtBu)]_2$ complex to deprotonate **LH** as internal base yielding Ir species **1**. Route *B* shows the direct mixing of all reagents to yield the Rh species **2**.

The analogous rhodium complex **2** was obtained in 45% yield using a slightly different synthetic method, in which the imidazolium salt, the base, and the $[Rh(cod)Cl]_2$ metal precursor were mixed directly in dichloromethane (route *B*).

Endeavors to remove the chloride ligand from the [M(cod)-Cl(κ^1*C*-{C^{NHC}-NH_2})] complexes **1** and **2** with silver salts, in attempts to synthesize [M(cod)Cl(κ^2*C,N*-{C^{NHC}-NH_2})] complexes with bidentate coordination modes of neutral ligand **L*H***, proved unsuccessful and led to several side reactions.

Crystals of both **1** and **2**, suitable for X-ray diffraction, were grown from slow vapor diffusion of pentane into a THF solution. The solid-state structure of **1**, which is isostructural with **2**, is shown in Figure 2. The solid-state structure shows a square -planar geometry around the metal center, with the cod ligand, a chloride, and the C^{NHC}-NH_2 ligand coordinated. One of the hydrogen atoms of the amine is directed toward the chloride, forming an intramolecular hydrogen bond (H···Cl 2.57(3) Å for Ir and 2.59(2) Å for Rh). As expected,[16−18] the distance from the metal to the centroid of the cod alkene bonds is longer for that trans to the NHC (2.0747(14) Å for Ir and 2.1071(10) Å for Rh) than for that trans to Cl (1.9862(14) Å for Ir and 1.9945(10) Å for Rh). This is ascribed to the greater trans influence of the NHC, reducing both σ-bonding and π-back-bonding interactions between the metal and the olefin ligand. This is also seen in the C=C bond lengths: the C=C bond trans to the NHC is shorter (1.395(3) Å for Ir and 1.377(2) Å for Rh) than that trans to the chloride (1.421(3) Å for Ir and 1.4068(19) Å for Rh).

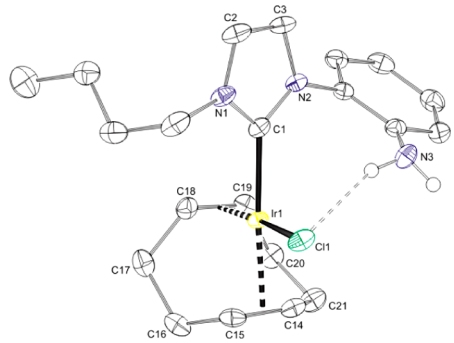

Figure 2. Displacement ellipsoid plot of Ir compound **1** in the crystal, drawn at the 50% probability level. C−H hydrogen atoms are omitted for clarity. The intramolecular hydrogen bond is indicated with a thin dashed line. Rh compound **2** is isostructural with **1**. The NH_2 group is pyramidal, with angle sums of 336(3)° in **1** and 338(3)° in **2**.

Complexes **1** and **2** were further characterized in solution using ^{1}H NMR spectroscopy. The cod signals of both species resonate at the expected shifts. The NH_2 signal at δ 4.35 ppm is not visibly split (as was seen for the half-sandwich complexes reported previously),[6] even though in the crystal packing it is clear that one of the hydrogens of the amine is involved in a hydrogen-bonding interaction with the chloride ligand. In Ir species **1** there are two NCH_2 signals centered around 4.59 and 4.35 ppm (the latter overlapping with the NH_2 signal), showing a complicated splitting pattern: a doublet of doublets of doublets (J = 13.5, 9.6, 6.0 Hz). This confirms that the NCH_2 protons are diastereotopic, since the molecule itself is chiral and rotation around the M−carbene bond is slow on the NMR time

dx.doi.org/10.1021/om5003599 | *Organometallics* 2014, 33, 2853−2861

scale. This pattern is also observed for Rh species **2**, where the NCH_2 protons resonate around 4.85 and 4.39 ppm.

Synthesis of [M(cod)Cl(κ^2*C*,*N*-{C^{NHC}-NH})] (M = Ir, Rh) Complexes 3 and 4. Reaction of both [Ir(cod)Cl(κ^1*C*-{C^{NHC}-NH_2})] complex **1** and [Rh(cod)Cl(κ^1*C*-{C^{NHC}-NH_2})] complex **2** with another 1 equiv of KO*t*Bu successfully resulted in deprotonation of the amine and substitution of the chloride ligand by the amido ligand thus formed. The ligand now coordinates in an anionic fashion (see Scheme 2), giving [M(cod)(κ^2*C*,*N*-{C^{NHC}-NH})] (M = Rh, Ir) complexes of general structure **II** (Figure 1).

Scheme 2. Formation of [M(cod)(κ^2*C*,*N*-{C^{NHC}-NH})] Complexes 3 and 4 (M = Ir, Rh)[a]

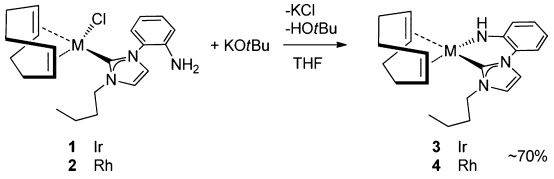

[a]Formation of [M(cod)(κ^2*C*,*N*-{C^{NHC}-NH})] complexes **3** and **4** (M = Ir, Rh) via reaction with KO*t*Bu, resulting in coordination of the C^{NHC}-NH_2 ligand in a deprotonated, bidentate fashion.

Even more than the starting materials, the deprotonated species are very prone to decomposition and we were unable to grow crystals for X-ray diffraction studies. The successful formation of complexes **3** and **4** was supported by ESI^+-MS measurements showing the $[M + H]^+$ peak, and the identity of the complexes was further established via NMR spectroscopy. The ^{1}H NMR spectra showing the formation of **4** from **2** are shown at the top and middle in Figure 3.

The presumed coordination of the amido moiety after deprotonation was confirmed with ^{1}H NMR spectroscopy, showing that the diastereotopic NCH_2 protons become more equivalent (see Figure SI-1 in the Supporting Information for the ^{1}H NMR spectra following the reaction of Ir complex **1** to **3**): in both **3** and **4** the two doublet of doublets of doublets stemming from the diastereotopic NCH_2 protons in **1** and **2** (and their neighboring protons) transform into a triplet. In addition, the signals for the alkyl substituent and the cod ligand become more defined. In the aromatic region a downfield shift of one the backbone protons of the imidazole and part of the aryl protons is seen and one signal of an aromatic proton shifts upfield, indicating delocalization of the charge created by deprotonation of the amine over the aromatic π system of the ligand. This behavior is seen for both complexes **3** and **4**. The reversibility of this deprotonation was established by adding another equiv of HCl to the somewhat more robust [Rh(cod)Cl(κ^2*C*,*N*-{C^{NHC}-NH})] species **4** (see Scheme 3 and Figure 3).

Scheme 3. Reversibility of (De)protonation of 2 and 4[a]

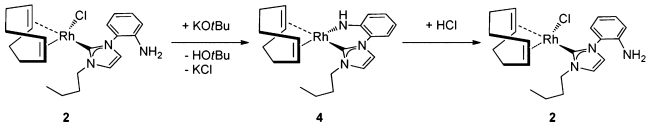

[a]Reversibility of (de)protonation of complex [Rh(cod)Cl(κ^1*C*-{C^{NHC}-NH_2})] **2** to **4** and vice versa. Reactions were performed in THF.

DFT Optimized Geometries of the Cationic [M(cod)Cl(κ^2*C*,*N*-{C^{NHC}-NH_2})]$^+$ and Neutral [M(cod)Cl(κ^2*C*,*N*-{C^{NHC}-NH})] Complexes (M = Ir, Rh). To properly explore the effect of the negative charge introduced upon ligand deprotonation at the amine donor on the geometrical and intraligand structural parameters of the rhodium and iridium complexes, we need to compare the geometries of the cationic

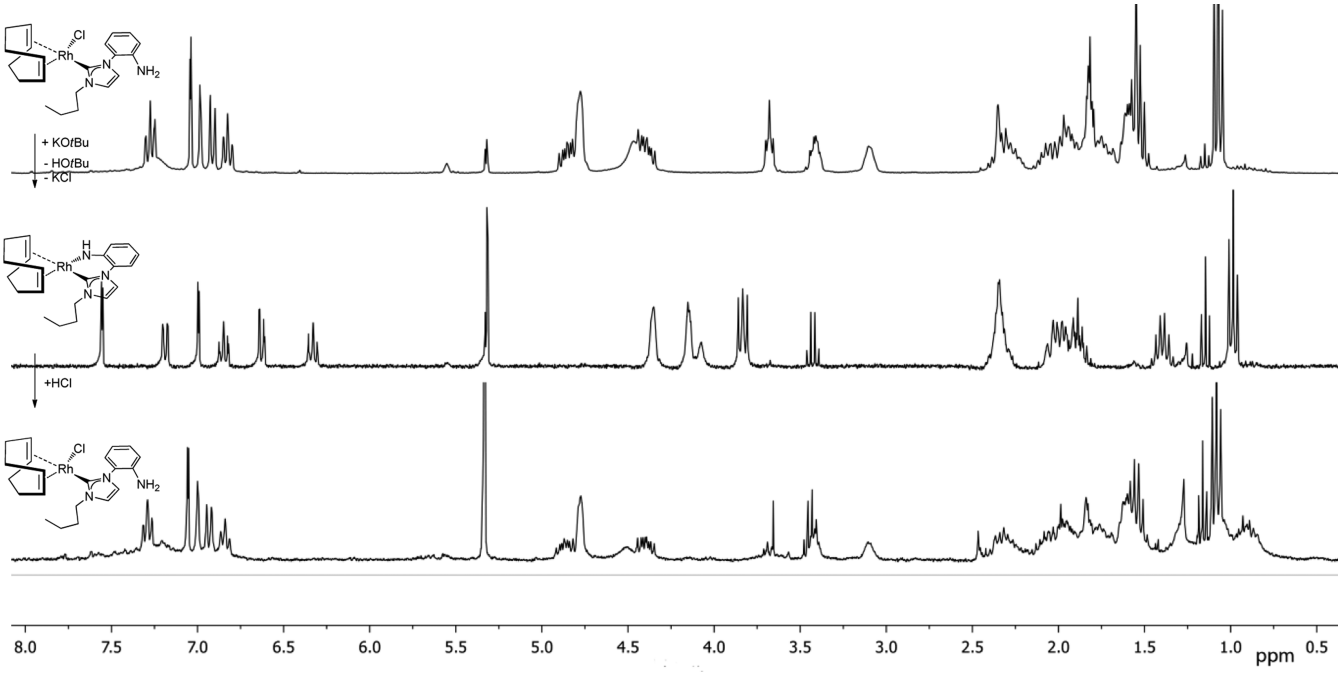

Figure 3. Reversibility experiment for Rh(cod)Cl(κ^2*C*,*N*-{C^{NHC}-NH_2}). Starting complex **2** (top) was deprotonated by KO*t*Bu, forming **4** (middle), and then converted back into the original complex **2** using HCl (bottom). The reactions were performed in THF, and after workup, measurements were performed in CD_2Cl_2.

dx.doi.org/10.1021/om5003599 | *Organometallics* 2014, 33, 2853−2861

$[M(cod)Cl(\kappa^2C,N\text{-}\{C^{NHC}\text{-}NH_2\})]^+$ species (M = Rh, Ir; general structure **I**) directly with those of the neutral $[M(cod)Cl(\kappa^2C,N\text{-}\{C^{NHC}\text{-}NH_2\})]$ complexes **3** and **4** (M = Rh, Ir; general structure **II**). However, it proved difficult to grow crystals of complexes **3** and **4** suitable for X-ray diffraction, and attempts to synthesize the elusive $[M(cod)Cl(\kappa^2C,N\text{-}\{C^{NHC}\text{-}NH_2\})]^+$ species wherein the neutral ligand ***L*H** coordinates in a bidentate fashion led to complex mixtures. Therefore, we had to resort to DFT calculations. For a proper comparison, we thus optimized the geometries of both the elusive cationic $[M(cod)Cl(\kappa^2C,N\text{-}\{C^{NHC}\text{-}NH_2\})]^+$ species and the synthesized neutral $[M(cod)Cl(\kappa^2C,N\text{-}\{C^{NHC}\text{-}NH\})]$ species **3** and **4** with DFT, using the same functional and basis set. First we looked at the calculated geometry of complexes **3** and **4** (see Figure 4). The two structures exhibit similar geometries,

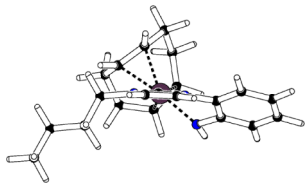

Figure 4. Calculated $[Ir(cod)(\kappa^2C,N\text{-}\{C^{NHC}\text{-}NH\})]$ structure **3** from a side-on view. The chelate ring that is formed by the $C^{NHC}\text{-}NH_2$ ligand can be seen to twist slightly out of plane. Ir complex **3** is isostructural with Rh complex **4**.

where the aryl ring is only twisted slightly out of plane with the NHC in comparison to **1** and **2**, due to coordination of the amine. The difference in torsion angles of the $N^{NHC}\text{–}C^{NHC}\text{–}M\text{–}N$ plane is negligible: in the case of Ir complex **3** calculations indicate a torsion angle of 32.6° and in the case of the Rh complex **4** a torsion angle of 35.4°. Rotation of the *n*Bu group, which is accompanied by a smaller torsion angle and therefore a more planar structure, has a very low energy barrier (between 0.3 and 0.6 kcal mol^{-1}).

To continue the structural investigations, we analyzed the calculated bond distance changes on going from the general structure **I** to that of **II**, for both iridium and rhodium (see Figure 5). Calculated bond lengths (see Table 1) show that, upon deprotonation, the monoanionic charge becomes delocalized over the ring system for both the iridium and rhodium structures.

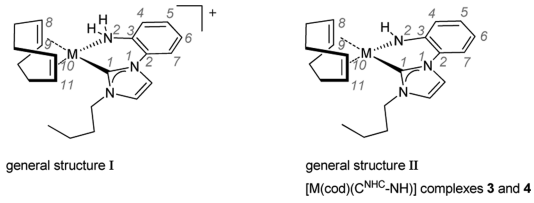

Figure 5. Atom-numbering scheme used to report the results from the DFT calculations regarding structures **I** and **II**.

This delocalization can be concluded from the fact that the C–C bonds of the phenyl ring become inequivalent, showing alternate lengthening and shortening pointing to partial "dearomatization". In addition, the C-NH bond (C3–N2) becomes shorter.

This means that there is a significant contribution of the charge delocalized resonance structure shown in Scheme 4, thus revealing the conjugating properties of the NHC-aniline motif. Several other anticipated properties become apparent from the calculations. In the calculated $[M(cod)(\kappa^2C,N\text{-}\{C^{NHC}\text{-}NH_2\})]^+$ structures the M–alkene bond distance (measured from the centroid of the cod C=C bond) trans to the NHC is longer than the M–alkene bond trans to the amine, due to the stronger trans influence of the carbene, which is in accordance with the literature.[16,17] Upon deprotonation the M–C(cod) distances (from the metal to the center of the alkene bond) trans to the NHC become a bit shorter, while the distances of the M–C(cod) bonds trans to the NH moiety stay the same (see Table 1). This is probably caused by strong π back-donation to the olefin trans to the amine donor, which induces a stronger metal–olefin interaction.

Synthesis of Bis-Ru(III) Complex 5 Containing Two Coordination Modes of the $C^{NHC}\text{-}NH_2$ Ligand. In addition to the Rh and Ir complexes described above, we also attempted to investigate coordination of the $C^{NHC}\text{-}NH_2$ ligand ***L*H** to Ru(cod) precursors. While the Ru(cod) precursors $[Ru(cod)Cl_2]_n$ and $[Ru(cod)Cl_2(MeCN)_2]$ are easily accessible, no reports on the existence of Ru(cod)(NHC) complexes have been disclosed, let alone Ru(cod) complexes with a chelating NHC-amine ligand. Our synthetic attempts seem to confirm that such complexes are indeed difficult to prepare.

A multitude of attempts involving different precursors ($[Ru(cod)Cl_2]_n$, $[Ru(cod)Cl_2(MeCN)_2]$, $[RuCp^*(cod)Cl]$), bases (KO*t*Bu, NaH, NaHMDS), approaches (ligand deprotonated, deprotonated in situ or via silver complex), solvents, additives, and reaction conditions were attempted. In almost all cases, an inseparable or decomposed product mixture was found, and in many cases the cod signals were missing. In the end, isolation of a $[Ru(cod)(C^{NHC}\text{-}NH_2)]$ species proved unsuccessful in our hands. However, the route depicted in Scheme 5 did result in the formation of an isolable complex, which proved to be the bis-ligated dinuclear complex **5**, lacking cod ligands.

$[Ru(cod)Cl_2]_n$ was refluxed in MeOH with 1.2 equiv of NaH for 60 min, and after subsequent addition of 1 equiv of ligand ***L*H** the solution was refluxed under an atmosphere of N_2 overnight. Workup yielded a dark green solid in ~50% yield, characterized as $[\{Ru(\kappa^2C,N\text{-}\{C^{NHC}\text{-}NH\})(\kappa^2C,N\text{-}\{C^{NHC}\text{-}NH_2\})Cl\}_2(\mu\text{-}Cl)]PF_6$ (**5**). The green color indicated oxidation of ruthenium(II) to ruthenium(III). This could be due to contact of the solution with air/oxygen. A controlled amount of oxygen is apparently crucial, since completely excluding O_2 from the reaction mixture does not result in a dark green solid and opening the solution to a substantial amount of air resulted in very low yields (~5%).

Crystals of **5** suitable for X-ray diffraction were obtained from slow vapor diffusion of cyclohexane into a THF solution. The solid-state structure of the product is shown in Figure 6. It reveals several unusual features.

The first feature is that the obtained structure, in agreement with the green color, indeed contains two (octahedral) ruthenium(III) centers. Second, there are two different bidentate ligands coordinated to each ruthenium center: the neutral bidentate $C^{NHC}\text{-}NH_2$ ligand ***L*H** (with both the NHC and amine donor coordinating) and the monoanionic bidentate $C^{NHC}\text{-}NH^-$ ligand $\mathbf{L}^-$ (with both the NHC and the amido donor coordinating).

The alkyl tails of both ligands point to the same face, as the anilines do. Additionally, the NH_2 moieties form hydrogen bonds to the chlorides coordinating to the other ruthenium center, and both ruthenium centers are further connected via

dx.doi.org/10.1021/om5003599 | *Organometallics* 2014, 33, 2853–2861

Table 1. Selected Calculated Bond Length Changes of the DFT Optimized Geometries of $[Ir(cod)(C^{NHC}\text{-}NH_2)]^+$ to $Ir(cod)(C^{NHC}\text{-}NH)$ and of $[Rh(cod)(C^{NHC}\text{-}NH_2)]^+$ to $Rh(cod)(C^{NHC}\text{-}NH)$[a]

iridium				rhodium			
	bond length (Å)				bond length (Å)		
	I-NH_2	II-NH	difference (Å)[b]		I-NH_2	II-NH	difference (Å)[b]
Ir−C1	2.073	2.066	−0.007	Rh−C1	2.067	2.062	−0.006
Ir−N2	2.191	2.039	−0.152	Rh−N2	2.199	2.047	−0.152
C1−N1	1.375	1.373	−0.002	C1−N1	1.373	1.369	−0.004
N1−C2	1.426	1.426	0.000	N1−C2	1.426	1.427	0.001
C2−C3	1.400	1.417	0.017	C2−C3	1.401	1.420	0.019
C3−C4	1.387	1.417	0.030	C3−C4	1.388	1.419	0.031
C4−C5	1.391	1.379	−0.012	C4−C5	1.390	1.380	−0.010
C5−C6	1.387	1.395	0.008	C5−C6	1.388	1.396	0.008
C6−C7	1.390	1.386	−0.004	C6−C7	1.390	1.387	−0.003
C7−C2	1.389	1.394	0.005	C7−C2	1.389	1.391	0.002
C3−N2	1.452	1.358	−0.094	C3−N2	1.445	1.355	−0.090
Ir−(C8═C9)[b]	2.116	2.099	−0.017	Rh−(C8═C9)[b]	2.147	2.122	−0.025
Ir−(C10═C11)[c]	2.046	2.045	−0.001	Rh−(C10═C11)[c]	2.060	2.063	0.003
Ir−C8	2.213	2.229	0.016	Rh−C8	2.239	2.250	0.011
Ir−C9	2.242	2.195	−0.047	Rh−C9	2.270	2.214	−0.056
Ir−C10	2.163	2.129	−0.034	Rh−C10	2.176	2.139	−0.037
Ir−C11	2.164	2.199	0.035	Rh−C11	2.173	2.217	0.044

[a]Geometries optimized with Turbomole using the b3-lyp functional and the def2-TZVP basis set. [b]Difference in the respective bond lengths of the neutral and monoanionic ligand, calculated by (distance **II-NH**) − (distance **I-NH_2**). [c]M-(C8═C9) and M-(C10═C11) distances are measured to the centroid of the double bond.

Scheme 4. Contribution of the Delocalized Structure[a]

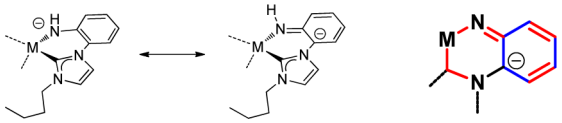

[a](left) Contribution of two main ligand resonance structures to intraligand charge delocalization in complexes **3** and **4**, showing the influence on the structural parameters of the ligand. (right) Influence of deprotonation on the structural parameters of the ligand. Bonds which become shorter are colored red, and bonds which become longer are colored blue.

Scheme 5. Synthesis of Bis-Ruthenium(III) Species 5[a]

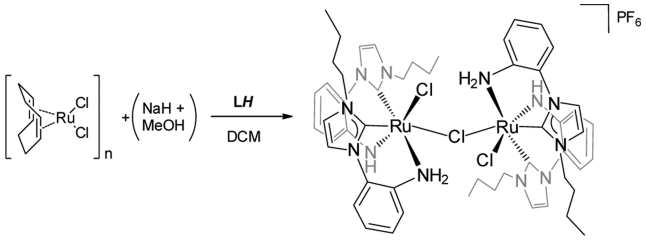

[a]Synthesis of bis-Ru(III) species **5** via $[Ru(cod)Cl_2]_n$ and $C^{NHC}\text{-}NH_2$ ligand **LH**.

one bridging chloride atom. The unit cell contains a PF_6^- anion, meaning that both ruthenium centers are in the oxidation state +III. The Ru−Cl−Ru angle is 130.11(2)°, which is quite large in comparison to reported literature values in the range between 70 and 100°.[19−22] Consequently, the Ru−Ru distance is also large (4.5700(4) Å) in comparison to the usual range between 3 and 4 Å. This is balanced by two intramolecular hydrogen bonds with H···Cl distances of respectively 2.57(3) and 2.45(3) Å between the halves of the

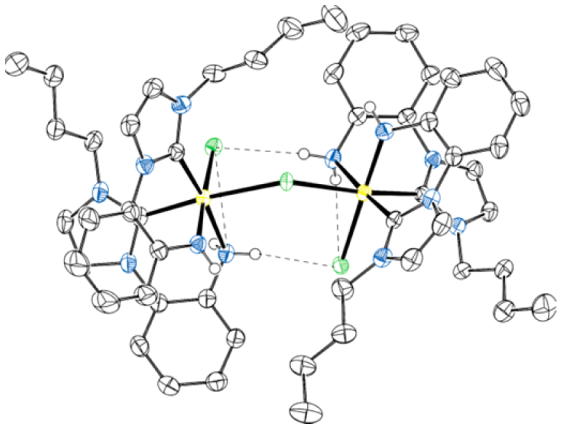

Figure 6. Displacement ellipsoid plot of Ru compound **5** in the crystal, drawn at the 50% probability level. C−H hydrogens, the PF_6^- anion, and THF solvent molecules are omitted for clarity. H bonds are indicated with dashed lines.

dimer, forming between an amine proton and a chloride on different Ru centers. Two other hydrogen bonds are also indicated, between the other amine proton and the chloride on the same Ru center.

The crystallographic data of Ru species **5** gave us the opportunity to directly compare the bond lengths and coordination modes of the neutral $C^{NHC}\text{-}NH_2$ ligand **LH** with those of the deprotonated monoanionic $C^{NHC}\text{-}NH^-$ ligand $\mathbf{L}^-$ in a single complex. The bond distances within the halves of the centrosymmetric dinuclear complex are identical. The data of the unique bond lengths are collected in Table 2 following the numbering scheme shown in Figure 7.

Within the NHC part of the ligand the bond lengths do not change much upon going from the neutral ligand **LH** to the deprotonated, monoanionic ligand $\mathbf{L}^-$. However, as observed for the calculated iridium and rhodium structures described

dx.doi.org/10.1021/om5003599 | Organometallics 2014, 33, 2853−2861

Table 2. Selected Bond Distances in the X-ray Crystal Structure of 5[a]

I-NH_2		II-NH		
	bond length (Å)		bond length (Å)	difference (Å)[b]
Ru1–N32	2.2098(19)	Ru1–N31	1.9576(19)	−0.252(3)
Ru–C12	2.002(2)	Ru–C11	2.007(2)	0.005(3)
C12–N12	1.379(3)	C11–N11	1.378(3)	−0.001(4)
N12–C42	1.429(3)	N11–C41	1.421(3)	−0.008(4)
C42–C92	1.402(3)	C41–C91	1.405(3)	0.003(4)
C82–C92	1.390(3)	C81–C91	1.404(4)	0.014(5)
C72–C82	1.388(3)	C71–C81	1.369(4)	−0.019(5)
C62–C72	1.384(4)	C61–C71	1.395(5)	0.012(6)
C52–C62	1.394(4)	C51–C61	1.372(4)	−0.022(6)
C42–C52	1.383(3)	C41–C51	1.395(3)	0.012(4)
C92–N32	1.429(3)	C91–N31	1,374(3)	−0.055(4)

[a]Structural parameters of **5** were obtained from the X-ray crystal structure. The numbering scheme is indicated on the half of the dimer shown in Figure 7. [b]Difference in the respective bond lengths of the neutral and monoanionic ligand, calculated by (distance **II-NH**) − (distance **I-NH_2**).

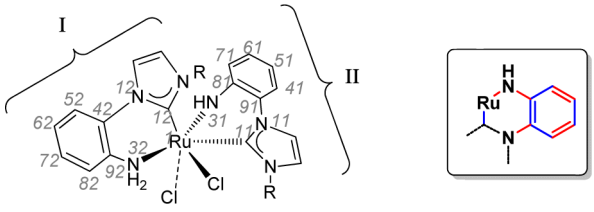

Figure 7. (left) Numbering scheme indicated on half of the dinuclear Ru complex **5**. (right) View showing which bonds become shorter (colored red) and longer (colored blue).

above, the anionic charge of ligand $\mathbf{L}^-$ has a clear inductive influence on the bond lengths of the aniline ring. Two resonance structures, illustrated in Scheme 4, contribute to the observed charge delocalization. The C–NH distance becomes shorter, two bonds in the aniline ring obtain more double-bond character, and the bond connecting the imidazole to the aniline also becomes shorter. Because of the charge, the NH–Ru distance also shortens. Indeed, the data from the solid-state structure suggest an influence of charge on the ligand structure similar to that found for the calculated general structures **I** and **II** for iridium and rhodium. However, considering the standard uncertainties in the bond length differences found in the solid-state structure, additional data are required to draw firm conclusions.

^{1}H NMR spectra of species **5** reveal very sharp signals in the normal chemical shift range between 0 and 10 ppm, implying that **5** is diamagnetic at room temperature in solution. Both ^{1}H and ^{13}C NMR (see Figure SI-3 in the Supporting Information for spectra) show a double set of signals originating from the alkyl substituents on the two types of coordinating ligands (**L*H*** and $\mathbf{L}^-$). The two signal sets of the alkyl substituents could not be unequivocally assigned as belonging to **L*H*** or $\mathbf{L}^-$. Both NCH_2 moieties of **5** are now diastereotopic, since both ligands coordinate in a bidentate fashion. In the aromatic region there are two signals that deviate significantly from the others. One is found resonating quite far upfield at 5.74 ppm, and one is found much further downfield, at 8.23 ppm. These signals seem to be shifted due to the shielding and deshielding effects between the two aniline rings. This indicates that the two ligands are still coordinated in the manner found in the solid state. Further identification of **5** was performed using HR-ESI MS, showing the presence of the $[M - PF_6]^+$ species in solution.

There are few literature examples of diamagnetic dinuclear Ru(III) complexes. Lahiri reports a structure where two Ru(III) centers are bridged via a noninnocent ligand.[23] Other examples have been given by Sudha (reporting a dinuclear tribridged oxo species)[24] and Wieghardt (reporting a disulfide-bridged species).[25] No reports have been found, however, on diamagnetic dinuclear Ru(III) structures bridged by chlorides, especially not ones bridged by one chloride and two hydrogen bonds. Therefore, this is the first report of such an exceptional species.

The diamagnetic nature of **5** is remarkable. The solid-state structure of **5** clearly reveals that the structure is built from two interacting d^5 low-spin ruthenium(III) centers, each containing an unpaired electron. Two possible explanations for the diamagnetic nature of **5** are plausible: (1) complex **5** is actually a delocalized mixed-valent Ru^{II}–Ru^{IV} species (closed-shell), and (2) the two Ru^{III} sites are (strongly) antiferromagnetically coupled (open-shell singlet). To shed more light on this matter, we performed some DFT calculations, shown in Table 3.

Table 3. Relative Energies of Different Spin States of Complex 5[a]

	$\langle S^2\rangle$[b]	energy (au)	rel energy (kcal mol^{-1})
closed-shell singlet	0	−4247.93811	0
open-shell singlet (uncorrected)	1.0209	−4247.97409	−22.578
open-shell singlet (spin corrected)		−4247.97410	−22.581
triplet	2.0209	−4247.97409	−22.575

[a]Geometries optimized with Turbomole using the b3-lyp functional and the def2-TZVP basis set. [b]Expectation value of the total spin.

Clearly, the closed-shell configuration is much higher in energy than both the triplet and the open-shell singlet configurations according to DFT. In agreement with the diamagnetic nature of **5**, the open-shell singlet configuration is indeed slightly lower in energy than the triplet. As such, the diamagnetic nature of **5** is best explained by antiferromagnetic coupling between the two unpaired electrons located at the ruthenium(III) sites. However, it remains to be noted that the open-shell singlet and triplet electronic structures are calculated to be (nearly) degenerate at the b3-lyp, def2-TZVP DFT level. A larger energy difference is expected for a strongly antiferromagnetically coupled system leading to diamagnetic behavior at room temperature in solution. Hence, we tentatively assume that the DFT calculated energy difference between the open-shell singlet and triplet electronic structures of **5** is underestimated.

dx.doi.org/10.1021/om5003599 | *Organometallics* 2014, 33, 2853–2861

CONCLUSIONS

We disclose monodentate and bidentate coordination modes of the neutral C_{NHC}-NH_2 ligand **L*H*** as well as bidentate coordination of (deprotonated) C_{NHC}-NH^- ligand $\mathbf{L}^-$ to Rh, Ir, and Ru: M(cod)Cl(C_{NHC}-NH_2) complexes **1** (M = Ir) and **2** (M = Rh), where the neutral **L*H*** coordinates in a monodentate fashion, and which upon treatment with KO*t*Bu adopt a bidentate coordination mode of the resulting monoanionic $\mathbf{L}^-$ to give complexes [M(cod)(κ^2*C*,*N*-{C_{NHC}-NH}] **3** (M = Ir) and **4** (M = Rh). Attempts to synthesize similar Ru(cod) complexes were not successful; instead, we synthesized the novel chloro-bridged bis-ligated dinuclear ruthenium complex [(Ru(κ^2*C*,*N*-{CNHC-NH})(κ^2*C*,*N*-{C_{NHC}-NH_2})Cl)$_2$(μ-Cl)]PF_6 (**5**), lacking cod. The complex contains both **L*H*** and $\mathbf{L}^-$, each coordinating to ruthenium(III) in a bidentate manner. The diamagnetic nature of complex **5** arises from antiferromagnetic coupling of the two low-spin ruthenium(III) centers through the chloride linker. Deprotonation of ligand **L*H*** to ligand $\mathbf{L}^-$ is reversible and has an impact on both the intraligand structural parameters and the coordination modes of these ligands to Rh, Ir, and Ru. The neutral ligand **L*H*** is only weakly chelating, and its nitrogen donor is apparently a weaker donor than a chloride ligand in the case of rhodium(I) and iridium(I). In ruthenium(III) complex **5** ligand **L*H*** does bind as a bidentate chelating ligand. As expected, the monoanionic (deprotonated) ligand $\mathbf{L}^-$ binds as a bidentate chelating ligand in all cases studied. Close inspection of the intraligand bond distances of chelating bidentate ligands **L*H*** and $\mathbf{L}^-$, using both the experimental bond lengths of ruthenium complex **5** and those from the DFT optimized [M(cod)(κ^2*C*,*N*-{C^{NHC}-NH_2})]$^+$ and [M(cod)(κ^2*C*,*N*-{C^{NHC}-NH})] (M = Rh, Ir) structures, suggest that the anionic charge of the $\mathbf{L}^-$ ligand is delocalized over the ligand π frame, mainly affecting the bond lengths of the anilido ring, partially entering the NHC moiety.

EXPERIMENTAL SECTION

General Remarks. All experiments were carried out under an atmosphere of purified nitrogen using standard Schlenk techniques. Solvents were freshly distilled under an argon atmosphere from sodium (toluene), sodium benzophenone ketyl (THF, pentane, and diethyl ether), and CaH_2 (cyclohexane, CH_2Cl_2, and MeCN). MeOH and *i*-PrOH were distilled from CaH_2 under a nitrogen atmosphere and were stored over 4 Å molecular sieves. Acetophenone was vacuum-distilled from CaH_2 under a nitrogen atmosphere and was stored over 4 Å molecular sieves. Deuterated solvents ($CDCl_3$ and CD_2Cl_2) were distilled from CaH_2 under a nitrogen atmosphere and stored over 4 Å molecular sieves. DMSO was purchased as the dry solvent. $[Rh(cod)Cl]_2$[26] and imidazole aniline[27] were prepared according to literature procedures. Other reagents were obtained commercially and used as received. NMR spectra were recorded on a 400, 300, or 500 MHz instrument. ^{1}H and ^{13}C{^{1}H} chemical shifts are reported in parts per million (δ, ppm) downfield from TMS, and ^{31}P{^{1}H} chemical shifts are reported in ppm downfield from 85% H_3PO_4. Abbreviations used in the reporting of NMR spectra are b = broad, s = singlet, d = doublet, t = triplet, q = quartet, and m = multiplet. High-resolution mass spectra were recorded on a four-sector mass spectrometer coupled to a data system for FAB measurements. High-resolution electrospray ionization mass spectra (HR-ESI MS) were recorded on a MicroTOFQ instrument in ESI positive mode, with capillary voltage 4.5 kV.

Preparation of 1-(2-Aminophenyl)-3-*n*-butylimidazolium PF_6 (C^{NHC}-NH_2; L*H*) Based on a Procedure from Ref 28. Imidazole aniline (0.72 gr, 4.54 mmol) was weighed in a pressure tube and suspended in 20 mL of MeCN. 1-Bromobutane (0.61 gr, 4.54 mmol) was added, and after the tube was sealed, the mixture was heated to 90 °C for 4 days. The mixture was then cooled to room temperature, and the volatiles were removed in vacuo. Purification was performed by dissolving the product in a small amount of MeOH and adding this solution dropwise to 200 mL of Et_2O. Light to dark brown solids were obtained. To exchange the bromide for a PF_6 anion, the product was stirred with an excess of KPF_6 (4.18 gr, 22.7 mmol) in 20 mL of CH_2Cl_2 overnight at room temperature. The salts were removed by filtration over a pad of Celite, and the product was dried in vacuo. In case an oily solid was obtained, a washing with Et_2O was performed and the product was obtained as a brown solid in 91% yield. ^{1}H NMR (300 MHz, CD_2Cl_2): δ 8.60 (s, 1H, im H), 7.48 (t, J = 1.6 Hz, 2H, im =CH), 7.36 (m, 1H, H_{Ar}), 7.18 (dd, J = 7.9, 1.4 Hz, 1H, H_{Ar}), 6.95 (d, J = 8.2 Hz, 1H, H_{Ar}), 6.90 (m, 1H, H_{Ar}), 4.32 (t, J = 7.5 Hz, 2H, NCH_2), 4.07 (bs, 2H, NH_2), 1.96 (m, 2H, CH_2), 1.45 (m, 2H, CH_2), 1.01 (t, J = 7.4 Hz, 3H) ppm. ^{19}F NMR (282 MHz, CD_2Cl_2): δ −72.95 (d, J = 711.3 Hz) ppm.

Preparation of [Ir(cod)Cl(κ^1*C*-{C^{NHC}-NH_2})] (1) Based on a Procedure from Ref 14. $[Ir(cod)Cl]_2$ (268 mg, 0.4 mmol) and KO*t*Bu (98 mg, 0.84 mmol) were dissolved in 7 mL of THF, and the solution was stirred for 1.5 h at room temperature. To this mixture was slowly added a solution of C^{NHC}-NH_2 ligand **L*H*** dissolved in 7 mL of THF (290 mg, 0.8 mmol), and the mixture was stirred at room temperature for 3 h. Subsequently, the THF solvent was evaporated in vacuo the residue was redissolved in 5 mL of DCM, and this solution was quickly filtered over Celite and dried in vacuo. A 5 mL portion of MeCN was added, and the mixture was cooled to −20 °C to precipitate the product, which was then collected and dried in vacuo to yield 53% of a yellow powder. Crystals suitable for X-ray diffraction were grown from slow diffusion of pentane into a THF solution. ^{1}H NMR (300 MHz, THF-d_8): δ 7.28 (d, J = 1.8 Hz, 1H, =CH), 7.22 (br, 1H, HAr), 7.15 (m, 2H, =CH and HAr), 6.81 (d, J = 8.0 Hz, 1H, HAr), 6.67 (m, 1H, HAr), 4.78 (br s, 2H, cod CH) 4.59 (ddd, J = 13.5, 9.6, 6.0 Hz, 1H, NCH_2), 4.35 (ddd, J = 13.2, 9.4, 6.2 Hz, 3H, NCH_2 and NH_2), 2.95 (br s, 1H, cod CH), 2.80 (br s, 1H, cod CH), 2.08 (m, 4H, cod CH_2), 1.92 (m, 2H, CH_2), 1.47 (m, 6H, CH_2 and cod CH_2), 1.03 (t, J = 7.4 Hz, 3H, CH_3) ppm. ^{1}H NMR (300 MHz, benzene-d_6): δ 7.03 (td, J = 8.1, 1.5 Hz, 1H, H_{Ar}), 6.82 (br s, 1H, H_{Ar}), 6.55 (t, J = 7.0 Hz, 1H, H_{Ar}), 6.37 (dd, J = 8.1, 1.3 Hz, 1H, H_{Ar}), 6.25 (d, J = 1.8 Hz, 1H, =C*H*), 6.13 (d, J = 2.0 Hz, 1H, =C*H*), 4.85 (bs, 2H, =C*H* cod), 4.52 (b, 2H, NH_2) 4.38 (ddd, J = 13.4, 9.6, 5.9 Hz, 1H, NCH_2), 4.10 (ddd, J = 13.4, 9.5, 6.1 Hz, 1H, NCH_2), 3.06 (bs, 1H, =C*H* cod), 2.98 (bs, 1H, =C*H* cod), 2.11(bs, 2H, NH_2), 1.94−1.69 (m, 3H, CH_2 cod), 1.66−1.32 (m, 5H, CH_2 cod), 1.17 (h, J = 7.6 Hz, 2H, CH_2) 0.82 (t, J = 7.3 Hz, 3H) ppm. ^{13}C NMR (75 MHz, benzene-d_6): δ 155.16 (s, C_q carbene), 147.69 (s, C_q), 129.66 (s, CH_{Ar}), 127.60 (s, CH_{Ar}), 126.50 (s, C_q), 122.85 (s, =CH), 119.81 (s, =CH), 117.51 (s, CH_{Ar}), 117.01 (s, CH_{Ar}), 84.35(s, CH cod), 83.44 (s, CH cod), 52.64 (s, CH cod), 51.37 (s, CH cod), 50.63 (s, NCH_2 ligand), 33.99 (s, CH_2 cod), 33.33 (s, CH_2 cod), 32.61 (s, CH_2 ligand), 29.66 (s, CH_2 cod), 29.38 (s, CH_2 cod), 19.95 (s, CH_2 ligand), 13.68 (s, CH_3 ligand) ppm. C-APT, CH, and COSY NMR spectroscopy has been used in the identification of the peaks. FAB$^+$-MS (CH_2Cl_2) for $C_{21}H_{29}N_3Ir$: m/z calculated 516.1992 (100%) [M − Cl]$^+$, observed 516.2000. Anal. Calcd for $C_{21}H_{29}ClIrN_3.H_2O$: C, 44.29; H, 5.49; N, 7.38. Found: C, 44.49; H, 5.47; N, 7.49.

Preparation of [Rh(cod)Cl(κ^1*C*-{C^{NHC}-NH_2})] (2) Based on a Procedure from Ref 29. $[Rh(cod)Cl]_2$ (140 mg, 0.28 mmol), KO*t*Bu (76 mg, 0.64 mmol), and C^{NHC}-NH_2 ligand **L*H*** (202 mg, 0.56 mmol) were weighed in a Schlenk tube and dissolved in 2 mL of THF and 10 mL of DCM. The mixture was stirred at room temperature for 4 h, after which all solvents were removed. The residue was redissolved in 5 mL of DCM, and the solution was filtered over a pad of Celite. After evaporation of the solvent a yellow-brown product remained. To this was added 8 mL of MeCN, and the mixture was cooled to −20 °C for 1 h to precipitate the product. The MeCN was removed and the yellow solid dried in vacuo (45% yield). ^{1}H NMR (300 MHz, CD_2Cl_2): δ 7.36−7.17 (m, 2H, H_{Ar}), 7.03 (d, J = 1.9 Hz, 1H, =C*H*), 6.97 (d, J = 1.7 Hz, 1H, =C*H*), 6.90 (m, 1H, H_{Ar}), 6.81 (t, J = 7.5 Hz, 1H, H_{Ar}), 4.85 (m, 1H, NCH_2), 4.77 (s, 2H, cod C*H*), 4.46 (bs, 2H, NH_2), 4.39 (m, 1H, NCH_2), 3.40 (br, 1H, cod C*H*), 3.09 (br, 1H, cod

dx.doi.org/10.1021/om5003599 | *Organometallics* 2014, 33, 2853−2861

CH), 2.48−1.88 (m, 6H, CH_2 and cod CH_2), 1.77−1.42 (m, 6H, CH_2 and cod CH_2), 1.06 (t, J = 7.4 Hz, 3H, CH_3) ppm. ^{13}C NMR (75 MHz, CD_2Cl_2): δ 143.11 (d, J = 54.9 Hz, C_q carbene), 130.24 (s, C_q), 129.15 (s, CH_{Ar}), 128.84 (s, CH_{Ar}), 127.16 (s, C_q), 123.97 (s, =CH), 121.07 (s, =CH), 118.15 (s, CH_{Ar}), 117.73 (s, CH_{Ar}), 98.08 (d, J = 7.43 Hz, CH cod), 97.44 (d, J = 7.00 Hz, CH cod), 70.05 (br, CH cod), 69.08 (br, CH cod), 51.75 (s, NCH_2 ligand), 33.79 (s, CH_2 cod), 33.37 (s, CH_2 cod), 32.49 (s, CH_2 ligand), 29.16 (d, J = 15.89 Hz, long-range interaction of this CH_2 with Rh, CH_2 cod), 28.56 (s, CH_2 cod), 20.76 (s, CH_2 ligand), 14.27 (s, CH_3 ligand) ppm. FAB$^+$-MS (CH_2Cl_2) for $C_{21}H_{29}N_3Rh$: m/z calculated 426.1417 (100%) $[M - Cl]^+$, observed 426.1416. Anal. Calcd for $C_{21}H_{29}ClN_3Rh.H_2O$: C, 52.54; H, 6.51; N, 8.76. Found: C, 52.14; H, 6.04; N, 8.85%.

Preparation of [Ir(cod)(κ^2*C*,*N*-{C^{NHC}-NH})] (3). Complex **1** ([Ir(cod)Cl(κ^1*C*-{C^{NHC}-NH_2})]; 10 mg, 0.018 mmol) and KO*t*Bu (2.4 mg, 0.02 mmol) were dissolved in 3 mL of THF, and the mixture was stirred in a Schlenk tube at room temperature for 30 min. The solution turned clear orange immediately. The solvent was evaporated, and the residue was redissolved in 5 mL of DCM and filtered over a pad of Celite. The filtrate was then again evaporated, and the product was washed with pentane and dried in vacuo to give a yellow-brown solid (±70% yield). ^{1}H NMR (500 MHz, THF-d_8): δ 8.02 (d, J = 2.1 Hz, 1H, =C*H*), 7.47 (d, J = 8.3 Hz, 1H, H_{Ar}), 7.30 (d, J = 2.1 Hz, 1H, =C*H*), 6.85 (m, 1H, H_{Ar}), 6.83 (dd, J = 8.1, 1.3 Hz, 1H, H_{Ar}), 6.38 (t, J = 7.3 Hz, 1H, H_{Ar}), 6.16 (bs, 1H, N*H*), 4.01 (m, 2H, cod C*H*), 3.89 (m, 2H, NCH_2), 3.71 (m, 2H, cod C*H*), 2.21 (m, 2H, cod CH_2), 2.10 (m, 2H, cod CH_2) 1.90 (m, 6H, cod CH_2 and CH_2), 1.38 (dq, J = 14.9, 7.4 Hz, 3H, CH_2), 0.96 (t, J = 7.4 Hz, 3H) ppm. ^{13}C NMR (75 MHz, CD_2Cl_2): δ 187.00 (s, C_q carbene), 155.75 (s, C_q), 130.24 (s, CH_{Ar}), 126.78 (s, CH_{Ar}), 126.30 (s, C_q), 123.49 (s, =CH), 120.93 (s, =CH), 118.79 (s, CH_{Ar}), 118.20 (s, CH_{Ar}), 83.52 (br, CH cod), 76.85 (br, CH cod), 66.22 (s, CH cod), 61.85 (s, CH cod), 50.63 (s, NCH_2 ligand), 35.06 (s, CH_2 cod), 33.38 (s, CH_2 cod), 30.26 (s, CH_2 cod), 29.56 (s, CH_2 cod), 28.56 (s, CH_2 ligand), 20.59 (s, CH_2 ligand), 14.18 (s, CH_3 ligand) ppm. HR-ESI MS for $C_{21}H_{28}IrN_3$: m/z calculated 516.1990 (100%) $[M + H]^+$, observed 516.1992.

Preparation of [Rh(cod)(C^{NHC}-NH)] (4). Complex **2** ([Rh(cod)-Cl(κ^1*C*-{C^{NHC}-NH_2})]; 46 mg, 0.1 mmol) and KO*t*Bu (14.6 mg, 0.12 mmol) were dissolved in 3 mL of THF, and the mixture was stirred in a Schlenk tube at room temperature for 30 min. The solvent was evaporated, and the residue was redissolved in 5 mL of DCM and filtered over a pad of Celite. The filtrate was then again evaporated, and the product was washed with pentane and dried in vacuo to yield a brown solid (±70% yield). ^{1}H NMR (500 MHz, THF-d_8): δ 7.81 (d, J = 2.0 Hz, 1H, =C*H*), 7.28 (d, J = 7.8 Hz, 1H, H_{Ar}), 7.25 (d, J = 2.0 Hz, 1H, =C*H*), 6.77 (ddd, J = 8.2, 7.0, 1.4 Hz, 1H, H_{Ar}), 6.62 (dd, J = 8.1, 1.4 Hz, 1H, H_{Ar}), 6.23 (ddd, J = 8.2, 7.0, 1.4 Hz, 1H, H_{Ar}), 4.37 (d, J = 2.4 Hz, 2H, cod C*H*), 4.34 (s, 1H, N*H*), 4.11 (d, J = 2.6 Hz, 2H, cod C*H*), 3.91 (m, 2H, NCH_2), 2.42−2.26 (m, 4H, cod CH_2), 2.08−2.02 (m, 2H, cod CH_2), 1.95 (m, 4H, cod CH_2 and CH_2), 1.43 (dq, J = 14.9, 7.4 Hz, 2H, CH_2), 1.03 (t, J = 7.4 Hz, 3H, CH_3) ppm. ^{13}C NMR (126 MHz, THF-d_8): δ 173.04 (d, J = 55.5 Hz, C_q carbene), 147.35 (s, C_q), 128.18 (s, CH_{Ar}), 125.71 (s, CH_{Ar}), 122.32 (s, C_q), 119.35 (s, =CH), 117.32 (s, =CH), 116.67 (s, CH_{Ar}), 109.64 (s, CH_{Ar}), 88.43 (d, J = 9.0 Hz, 2 x CH cod), 67.70 (d, J = 11.3 Hz, 2 × CH cod), 49.32 (s, NCH_2 ligand), 34.34 (s, CH_2 cod), 32.84 (s, CH_2 ligand), 28.73 (s, CH_2 cod), 27.83 (s, CH_2 cod), 19.80 (s, CH_2 ligand), 13.17 (s, CH_3 ligand) ppm. HMBC, HSQC, and C-apt NMR spectroscopy was used in the identification of the peaks. HR-ESI MS for $C_{21}H_{28}RhN_3$: m/z calculated 426.1416 (100%) $[M + H]^+$, observed 426.1417.

Preparation of [(Ru(κ^2*C*,*N*-{C^{NHC}-NH})(κ^2*C*,*N*-{C^{NHC}-NH_2})Cl)$_2$(μ-Cl)]PF_6 (5). $[Ru(cod)Cl_2]_n$ (280 mg, 1 mmol) was refluxed under N_2 in 10 mL of MeOH with NaH (24 mg, 1.1 mmol) for 60 min. Subsequently, ligand **L*H*** (361 mg, 1 mmol) was added and the mixture was refluxed overnight. The solid that was formed was separated from the blue solution via filtration and dried in vacuo. The product was then redissolved in 10 mL of DCM and filtered over a pad of Celite. Evaporating the solvent gave a dark green solid, which was washed with benzene and dried in vacuo (yield ∼50%). The amount of oxygen added appeared to be crucial, which hindered the reproducibility of the procedure. Crystals suitable for X-ray diffraction were grown by slow diffusion of cyclohexane into a THF solution. NMR: assignment of the signals below involves half of the centrosymmetric dinuclear complex. The two different alkyl-tail signals arising from the two ligands coordinated to one Ru center are not attributed to A or B due to ambiguity, only 1 to 4 (1 = CH_3 end, 4 = NCH_2). COSY NMR spectroscopy has been used in the identification of the peaks. ^{1}H NMR (300 MHz, CD_2Cl_2): δ 8.23 (d, J = 7.19 Hz, 1H, =C*H* or H_{Ar}), 8.02 (d, J = 9.66 Hz, 1H, NH_2), 7.50−6.75 (m, 10H, =C*H* and/or H_{Ar}), 5.74 (d, J = 7.71 Hz, 1H, =C*H* or H_{Ar}), 5.21 (m, 1H, NCH_2 (4)), 5.10 (d, J = 8.98 Hz, 1H, NH_2), 4.62 (m, 1H, NCH_2 (4)), 4.45 (bs, 1H, N*H*), 3.67 (m, 2H, CH_2 (4)), 2.59 (bs, 1H, H_2O interacting with N*H*), 2.18−1.79 (m, 2H, CH_2 (3)), 1.60 (m, 2H, CH_2 (2)), 1.46 (m, 2H, CH_2 (3)), 1.15 (m, 2H, CH_2 (2)), 1.01 (t, J = 7.34, 3H, CH_3 (1)), 0.92 (t, J = 6.94, 3H, CH_3 (1)) ppm. ^{13}C NMR (75 MHz, CD_2Cl_2): δ 169.88 (s, C_q carbene), 137.65 (s, C_{Ar} or =C*H*), 136.25 (s, C_{Ar} or =C*H*), 134.23 (s, C_{Ar} or =C*H*), 133.63 (s, C_{Ar} or =C*H*), 128.26 (s, C_{Ar} or =C*H*), 126.78 (s, C_{Ar} or =C*H*), 126.48 (s, C_{Ar} or =C*H*), 125.40 (s, C_{Ar} or =C*H*), 125.16 (s, C_{Ar} or =C*H*), 123.87 (s, C_{Ar} or =C*H*), 123.09 (s, C_{Ar} or =C*H*), 122.87 (s, C_{Ar} or =C*H*), 121.83 (s, C_{Ar} or =C*H*), 120.90 (s, C_{Ar} or =C*H*), 120.21 (s, C_{Ar} or =C*H*), 118.58 (s, C_{Ar} or =C*H*), 50.50 (s, NCH_2 ligand), 49.62 (s, NCH_2 ligand), 33.90 (s, CH_2 ligand), 32.43 (s, CH_2 ligand), 20.66 (s, CH_2 ligand), 20.26 (s, CH_2 ligand), 13.96 (s, CH_3 ligand), 13.69 (s, CH_3 ligand) ppm. One carbene signal was not found. ^{19}F NMR (282 MHz, CD_2Cl_2) δ −73.34 (d, J = 710.6 Hz). ^{31}P NMR (121 MHz, CD_2Cl_2): δ −144.49 (septet, J = 707.85 Hz) ppm. HR-ESI MS for $C_{52}H_{66}Cl_3N_{12}Ru_2$: m/z calculated 1167.2685 $[M - PF_6]^+$, observed 1167.2688.

DFT Calculations. Geometry optimizations were carried out with the Turbomole program package[30] coupled to the PQS Baker optimizer[31] via the BOpt package,[32] at the DFT/b3-lyp[33] level. We used the def2-TZVP basis set[34] (small-core pseudopotentials on Ru[35]) for the geometry optimizations. Scalar relativistic effects were included implicitly through the use of the Ir, Rh and Ru ECPs. All minima (no imaginary frequencies) were characterized by calculating the Hessian matrix. ZPE and gas-phase thermal corrections (entropy and enthalpy, 298 K, 1 bar) from these analyses were calculated.

The open-shell singlet electronic structure of **5** was evaluated employing the broken-symmetry protocol. The "real" energy ε_s of the (multideterminant) open-shell singlet species **5** was estimated from the ε_0 energies of the optimized single-determinant broken-symmetry solutions and the ε_1 energies from a separate unrestricted triplet (m_s = 1) calculations at the same geometry with the same functional and basis set, using the approximate spin correction formula proposed by Yamaguchi:[36]

$$\varepsilon_s \approx \frac{S_1^2\varepsilon_0 - S_0^2\varepsilon_1}{S_1^2 - S_0^2}$$

■ ASSOCIATED CONTENT

Supporting Information

Figures, tables, text, and CIF files giving X-ray structural data for compounds **1**, **2**, and **5**, Cartesian coordinates of the DFT optimized structures, NMR data for the deprotonation of **1** to **3**, the reversibility experiment between **2** and **4**, and details of the formation of **5**. This material is available free of charge via the Internet at http://pubs.acs.org.

■ AUTHOR INFORMATION

Corresponding Authors

*E-mail for B.d.B.: b.debruin@uva.nl.
*E-mail for C.J.E.: c.j.elsevier@uva.nl.

Notes

The authors declare no competing financial interest.

■ ACKNOWLEDGMENTS

Dr. Andreas Ehlers and Ing. Elwin Janssen of the VU University are kindly thanked for facilitating the exact ESI mass measurements. The X-ray diffractometer was financed by The Netherlands Organization for Scientific Research (NWO). This research was performed within the framework of the CatchBio program. The authors gratefully acknowledge the support of the Smart Mix Program of The Netherlands Ministry of Economic Affairs and The Netherlands Ministry of Education, Culture and Science.

■ REFERENCES

(1) De Frémont, P.; Marion, N.; Nolan, S. P. *Coord. Chem. Rev.* **2009**, *253*, 862−892.
(2) Wanzlick, H. W.; Schikora, E. *Angew. Chem.* **1960**, *72*, 494−494.
(3) Dragutan, V.; Dragutan, I.; Delaude, L.; Demonceau, A. *Coord. Chem. Rev.* **2007**, *251*, 765−794.
(4) Díez-González, S.; Marion, N.; Nolan, S. P. *Chem. Rev.* **2009**, *109*, 3612−3676.
(5) Sanford, M. S.; Ulman, M.; Grubbs, R. H. *J. Am. Chem. Soc.* **2001**, *123*, 749−750.
(6) Jansen, E.; Jongbloed, L. S.; Tromp, D. S.; Lutz, M.; de Bruin, B.; Elsevier, C. J. *ChemSusChem* **2013**, *6*, 1737−1744.
(7) Mindiola, D. J. *Angew. Chem., Int. Ed.* **2009**, *48*, 6198−6200.
(8) Bourget-Merle, L.; Lappert, M. F.; Severn, J. R. *Chem. Rev.* **2002**, *102*, 3031−3066.
(9) Watanabe, M.; Kashiwame, Y.; Kuwata, S.; Ikariya, T. *Eur. J. Inorg. Chem.* **2012**, *2012*, 504−511.
(10) Bouwkamp, M. W.; Lobkovsky, E.; Chirik, P. J. *Inorg. Chem.* **2006**, *45*, 2−4.
(11) Weintrob, E. C.; Tofan, D.; Bercaw, J. E. *Inorg. Chem.* **2009**, *48*, 3808−3813.
(12) O, W. W. N.; Lough, A. J.; Morris, R. H. *Organometallics* **2012**, *31*, 2137−2151.
(13) Field, L. D.; Messerle, B. A.; Vuong, K. Q.; Turner, P. *Organometallics* **2005**, *24*, 4241−4250.
(14) Song, G.; Wang, X.; Li, Y.; Li, X. *Organometallics* **2008**, *27*, 1187−1192.
(15) Herrmann, W. a. *Angew. Chem., Int. Ed.* **2002**, *41*, 1290−1309.
(16) Jong, H.; Patrick, B. O.; Fryzuk, M. D. *Can. J. Chem.* **2008**, *86*, 803−810.
(17) O, W. W. N.; Lough, A. J.; Morris, R. H. *Organometallics* **2013**, *32*, 3808−3818.
(18) Türkmen, H.; Pape, T.; Hahn, F. E.; Çetinkaya, B. *Eur. J. Inorg. Chem.* **2008**, *2008*, 5418−5423.
(19) Allardyce, C. S.; Dyson, P. J.; Ellis, D. J.; Salter, P. A.; Scopelliti, R. *J. Organomet. Chem.* **2003**, *668*, 35−42.
(20) Drouin, S. D.; Foucault, H. M.; Yap, G. P. A.; Fogg, D. E. *Organometallics* **2004**, *23*, 2583−2590.
(21) Waheed, A.; Jones, R. A.; Agapiou, K.; Yang, X.; Moore, J. A.; Ekerdt, J. G. *Organometallics* **2007**, *26*, 6778−6783.
(22) Salem, H.; Schmitt, M.; Herrlich (née Blumbach), U.; Kühnel, E.; Brill, M.; Nägele, P.; Bogado, A. L.; Rominger, F.; Hofmann, P. *Organometallics* **2013**, *32*, 29−46.
(23) Kar, S.; Sarkar, B.; Ghumaan, S.; Janardanan, D.; Van Slageren, J.; Fiedler, J.; Puranik, V. G.; Sunoj, R. B.; Kaim, W.; Lahiri, G. K. *Chem. Eur. J.* **2005**, *11*, 4901−4911.
(24) Sudha, C.; Mandal, S. K.; Chakravarty, A. R. *Inorg. Chem.* **1998**, *1669*, 270−278.
(25) Schneider, R.; Wieghardt, K.; Nuber, B. *Inorg. Chem.* **1993**, *32*, 4935−4939.
(26) Giordano, G.; Crabtree, R. H.; Heintz, R. M.; Forster, D.; Morris, D. E. *Inorg. Synth.* **1990**, *28*, 88−90.
(27) Blake, A. J.; Clark, B. a. J.; McNab, H.; Sommerville, C. C. *J. Chem. Soc., Perkin Trans. 1* **1997**, 1605−1608.
(28) Cross, W. B.; Daly, C. G.; Boutadla, Y.; Singh, K. *Dalton Trans.* **2011**, *40*, 9722−9730.
(29) Park, K. H.; Kim, S. Y.; Son, S. U.; Chung, Y. K. *Eur. J. Org. Chem.* **2003**, *2003*, 4341−4345.
(30) Ahlrichs, R. *Turbomole Version 6.5*; Theoretical Chemistry Group, University of Karlsruhe, Karlsruhe, Germany.
(31) *PQS version 2.4*; Parallel Quantum Solutions, Fayettevile, AK, USA, 2001. The Baker optimizer is available separately from PQS upon request: Baker, I. *J. Comput. Chem.* **1986**, *7*, 385−395.
(32) Budzelaar, P. H. M. *J. Comput. Chem.* **2007**, *28*, 2226−2236.
(33) (a) Lee, C.; Yang, W.; Parr, R. G. *Phys. Rev. B* **1988**, *37*, 785−789. (b) Becke, A. D. *J. Chem. Phys.* **1993**, *98*, 1372−1377. (c) Becke, A. D. *J. Chem. Phys.* **1993**, *98*, 5648−5652. (d) Calculations were performed using the Turbomole functional b3-lyp, which is not completely identical with the Gaussian B3LYP functional..
(34) (a) Weigend, F.; Ahlrichs, R. *Phys. Chem. Chem. Phys.* **2005**, *7*, 3297−3305. (b) Weigend, F.; Häser, M.; Patzelt, H.; Ahlrichs, R. *Chem. Phys. Lett.* **1998**, *294*, 143−152.
(35) (a) Turbomole basis set library, Turbomole Version 6.5.. (b) Andrae, D.; Haeussermann, U.; Dolg, M.; Stoll, H.; Preuss, H. *Theor. Chim. Acta* **1990**, *77*, 123−141.
(36) (a) Knijnenburg, Q.; Hetterscheid, D.; Kooistra, T. M.; Budzelaar, P. H. M. *Eur. J. Inorg. Chem.* **2004**, 1204. (b) Goldstein, E.; Beno, B.; Houk, K. N. *J. Am. Chem. Soc.* **1996**, *118*, 6036. (c) Yamanaka, S.; Kawakami, T.; Nagao, H.; Yamaguchi, Y. *Chem. Phys. Lett.* **1994**, *231*, 25.